EFFECTS OF COOLING RATES ON THERMAL PROFILES AND MICROSTRUCTURE OF ALUMINIUM 7075

A.H. Ahmad[1, 2, 3*], S. Naher[1, 2] and D. Brabazon[1, 2]

[1]School of Mechanical and Manufacturing Engineering,
Dublin City University, Dublin 9, Ireland
[*]Email: asnul@ump.edu.my
Phone : +609-424-2213 ; Fax : +609-424-2202
[2]Advanced Processing Technology Research Centre,
Dublin City University, Dublin 9, Ireland
[3]Faculty of Mechanical Engineering, Universiti Malaysia Pahang,
Pekan, Pahang, Malaysia

ABSTRACT

This paper presents the effects of different cooling rates on thermal profiles and microstructures of aluminum 7075. The 7075 alloy was heated in a graphite crucible to 750°C. In the experimental work two thermocouples were used to record the temperatures at the center and 30mm from the center of the graphite crucible. A slow cooling rate condition was achieved by placing the crucible into a chamber with Kaowool insulation. A higher cooling rate was achieved by placing the crucible in open atmosphere with controlled air flow over the crucible. The slow and high cooling rates were 0.03°C/s and 0.4°C/s respectively. The Data Acquisition (DAQ) system implemented using LabVIEW software was used to record the temperature-time profiles. The enthalpy of phase change at each temperature was estimated from the cooling curves. The changes of cooling rate were directly related to phase transformation including at liquidus, eutectic and solidus temperatures. The dendritic coherency point (DCP) was determined from analysis of the temperature difference between two thermocouples. The formation of DCP was found to be delayed with use of the slow cooling rate. DCP occurred at 615.2°C (0.75 fraction solid) for the slow cooling rate and at 633.1°C (0.3 fraction solid) for the higher cooling rate. The microstructure features were also found to alter significantly with the different cooling rates used. The microstructure was more spheroidal for the slow cooling rate compared with the higher cooling rate.

Keywords: Semi-solid metal; thermal profile; aluminum 7075; dendritic coherency point; spheroidal microstructure.

INTRODUCTION

In recent years, there has been an increasing interest in producing near-net-shape products with semi-solid metal (SSM) forming routes. This offers production with fewer porosity defects, lower filling time and no hot tearing problems. In addition, it allows for increased productivity that contributes to savings of production cost per unit. Since the discovery of SSM behavior in 1971, with the understanding of viscosity reduction within the semi-solid state upon shearing, the technology has advanced significantly(Spencer, Mehrabian, & Flemings, 1972; Yang, Moa, & Song, 2014).

Mechanical stirring using rotating impellers was used to produce laboratory scale feedstock production (Brabazon, Browne, & Carr, 2003; Hongwei Zhang & Lina Guan, 2010). Later, electromagnetic stirring was introduced to overcome the contact between agitator and metal, which required high energy consumption (Zoqui, Paes, & Es-Sadiqi, 2002). It uses an electromagnetic field for melting material and moving the metal fluid from one location to another. It was found that a fine structure of 30μm was produced with this technique (Kirkwood, 1994). The enhancement of the technology continued with the introduction of new thermal methods that produced fine microstructure features. The melt was rapidly solidified and held for a short period of time in the semi-solid temperature range to retard the formation of microstructure. The special characteristic of SSM is the occurrence of globular or spherical microstructure compared with the dendritic microstructure of the conventional process. The rounded microstructure helps material forming by giving more flexibility for microstructure movement. Solid grains rotate, slip and move as force is applied during processing (Kiuchi, 2002). This special characteristic allows SSM processing to be used in order to produce complex component geometries. An important metallurgical characteristic that has a significant effect during SSM processing is fraction solidity. Research shows that it is important to obtain a low viscosity and high fraction solids in SSM processing (Kiuchi, 2002). The low viscosity component helps material to flow inside the cavity and high fraction solids helps to prevent various defects, and provide a finer internal structure and high quality products. Previous studies have reported fraction solidity for SSM processing in the range of 30 to 70% (Vaneetveld, Rassili, Pierret, & Lecomte-Beckers, 2010).

Differential thermal analysis (DTA) and differential scanning calorimetry (DSC) are among the list of thermal analysis methods. Both of these techniques use a reference sample and a tested sample. The changes in energy and temperature between samples during testing were measured. DTA measures the temperature difference, and DCS gauges the energy difference between both samples. Another thermal analysis techniques uses two thermocouples to measure heat change in a single sample (Bäckerud, Chai, & Tamminen, 1991). This technique gives in-situ measurement and reflects the actual heat change in a test sample. It also provides useful information about the dendritic coherency point (DCP) that is important for SSM processing. DCP is the point where the strength of the material begins to develop (Farahany et al., 2012). At this point the dendrites start to impinge on one another across the solidification systems where the solidifying metal has negligible shear strength before DCP, compared to after this point of coherency when a dendritic network has formed. This point is consequently supplemented with increased system viscosity and strength. The use of aluminum 7075 in SSM processing has recently been investigated. Tensile properties of thixoformed 7075 processed with recrystallization and partial melting (Box) were better than those processed via the cooling slope route (Vaneetveld et al., 2010). Research also indicated that by selecting the proper processing parameters, yield strength was increased and part defect was reduced. The mechanical properties of 7075 feedstock were improved when prepared with combinations of low superheat pouring with a shear field (LSPSF), rheoforming process and T6 heat treatment (Guo, Yang, Wang, Hu, & Zhu, 2010). Among the advantages of this combined technique were that hot tearing defect and grain size decreased and density increased. The mechanical properties were also improved by using another technique called the thixoextrusion process, in comparison with as-received material (Guan et al., 2012). Recently, researchers have shown an increasing interest in processing 7075 within a semi-solid state because the properties of

this alloy are superior to conventional cast alloy. However, this alloy is difficult to process within the semi-solid state because it has narrow solidification ranges and a higher propensity for hot tearing. Although extensive research has been carried out on 7075, less attention has been given to detailed experimental investigation of the thermal profiles and microstructure at various solidification rates. The objective of the experimental work presented in this paper is to understand the relationship between the solidification rate, metallurgical behavior, and fraction phase evolution. The liquidus, eutectic, solidus temperatures, fraction solid, dendritic coherency point, and microstructure for different cooling rates were determined.

EXPERIMENTAL PROCEDURE

The chemical composition of the starting material used in this work, as determined by an Oxford Instrument Arc Spectrometer, is presented in Table 1. A schematic of the experimental set-up for a slow cooling rate is shown in Figure 1. A graphite crucible with 100mm diameter and 100mm height was used in this experiment. A 1kg 7075 billet was placed in the crucible and heated to a temperature of 750°C $\pm$ 5 °C using a Carbolite 1600 box furnace. The crucible was then transferred into the Kaowool chamber in order to achieve a slow cooling rate, or was placed in a forced air flow for a higher cooling rate. The specially designed chamber with Kaowool insulation contained 100mm of Kaowool beneath the crucible, 50mm side walls, and a 40mm thick top layer of Kaowool in order to ensure very slow cooling. Chromel-alumel K-type thermocouples were located at two different locations, one at the center of the crucible and one 35mm from the center closer to the crucible wall. Both thermocouples were immersed within the metal to a depth of 45mm from the top of the melt.

Table 1. The chemical composition of the aluminum 7075 (in wt %).

Aluminum 7075	Cr	Cu	Fe	Mg	Mn	Si	Ti	Zn	Al
	0.20	2.02	0.24	2.38	0.12	0.14	0.09	6.04	Bal

The temperature versus time cooling curve data was recorded using an NI PCI-6036E data acquisition (DAQ) card with cold junction compensation. After the cooling curves were captured, the cooling rates were calculated from the portion of the cooling curve below the solidus temperature (between 50 °C and 150 °C below the solidus temperature). A series of programs developed in LabVIEW allowed control of data acquisition rate, as well as calculation of the cooling curve differential (dT/dt curves) and fraction solid with respect to time. The DAQ rate was set to 500 Hz in order to allow sufficient data capture. For the slow cooling rate conditions this equated to 4,500,000 data points captured during the experiment period of two and a half hours. For the higher cooling rate conditions, there were approximately 583,000 data points captured (19 minutes). A base line was constructed on the dT/dt curves to represent the cooling rate which would have occurred in the absence latent heat evolution. The area between this curve and the actual cooling curve differential was calculated at each time point and divided by the total area between these curves in order to determine the fraction solid versus time curves, as per Eq. (1):

$$f_s = \frac{\int_{t_0}^{t_1} dH}{\int_{t_0}^{t_f} dH} = \frac{\int_{t_0}^{t_1} \left[\left.\frac{dT}{dt}\right|_{cc} - \left.\frac{dT}{dt}\right|_{bc} \right] dt}{\int_{t_0}^{t_f} \left[\left.\frac{dT}{dt}\right|_{cc} - \left.\frac{dT}{dt}\right|_{bc} \right] dt} \tag{1}$$

where f_s is the fraction solid present at a given time t_1, H is the latent heat, T is the temperature, $\left.\frac{dT}{dt}\right|_{cc}$ is the rate of change of the cooling curve and $\left.\frac{dT}{dt}\right|_{bc}$ is the rate of change of the base line curve volume.
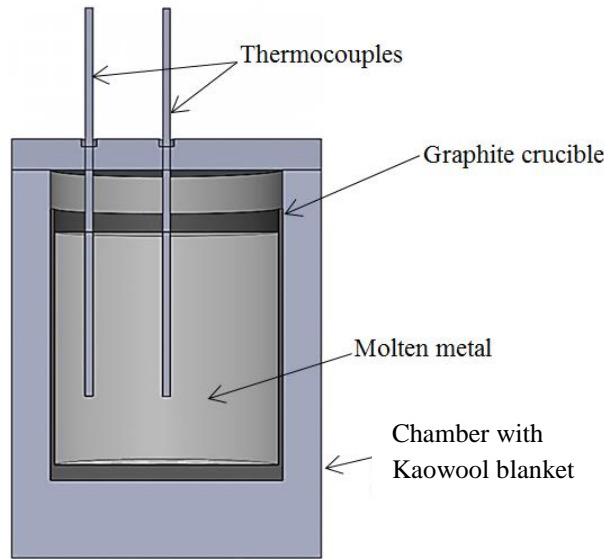
Figure 1. Schematic view of thermal analysis experimental set-up for slow cooling.

Separately, the temperature recorded from the thermocouple at the crucible wall was subtracted from the temperature reading from the center thermocouple at each given time. This temperature difference was plotted against time. The DCP was then determined by identifying the maximum absolute difference between these two readings.

Samples from the starting material and solidified alloy were cut at three different locations. The samples were mounted in Bakelite and were ground using 240, 600, and 1200 grit paper, polished using 9μm and given a final polish to 0.5μm using diamond paste. The samples were then etched using Keller's etch. A Reichert MeF2 universal camera optical microscope was used to view the microstructures. Buhler OmniMet Enterprise software was then used to capture the microstructure images.

RESULTS AND DISCUSSION

Thermal Analysis

The cooling curve and first derivate with baseline results for a cooling rate of 0.03°C/s (slow cooling) and 0.4°C/s (higher cooling) are presented in Figure 2 (a) and Figure 2 (b) respectively. The vertical lines in both figures indicate the liquidus and solidus temperature representing the starts and ends of solidification. The area within these vertical lines (liquidus and solidus) towards the first derivative line was calculated using

Eq. (1) for fraction solid estimation. The liquidus, eutectic and solidus temperature for the slow cooling rate were at 639.9°C, 470.2°C and 467.6°C meanwhile for the higher cooling rate were at 643°C, 482.7°C and 479.2°C respectively.

(a)

(b)
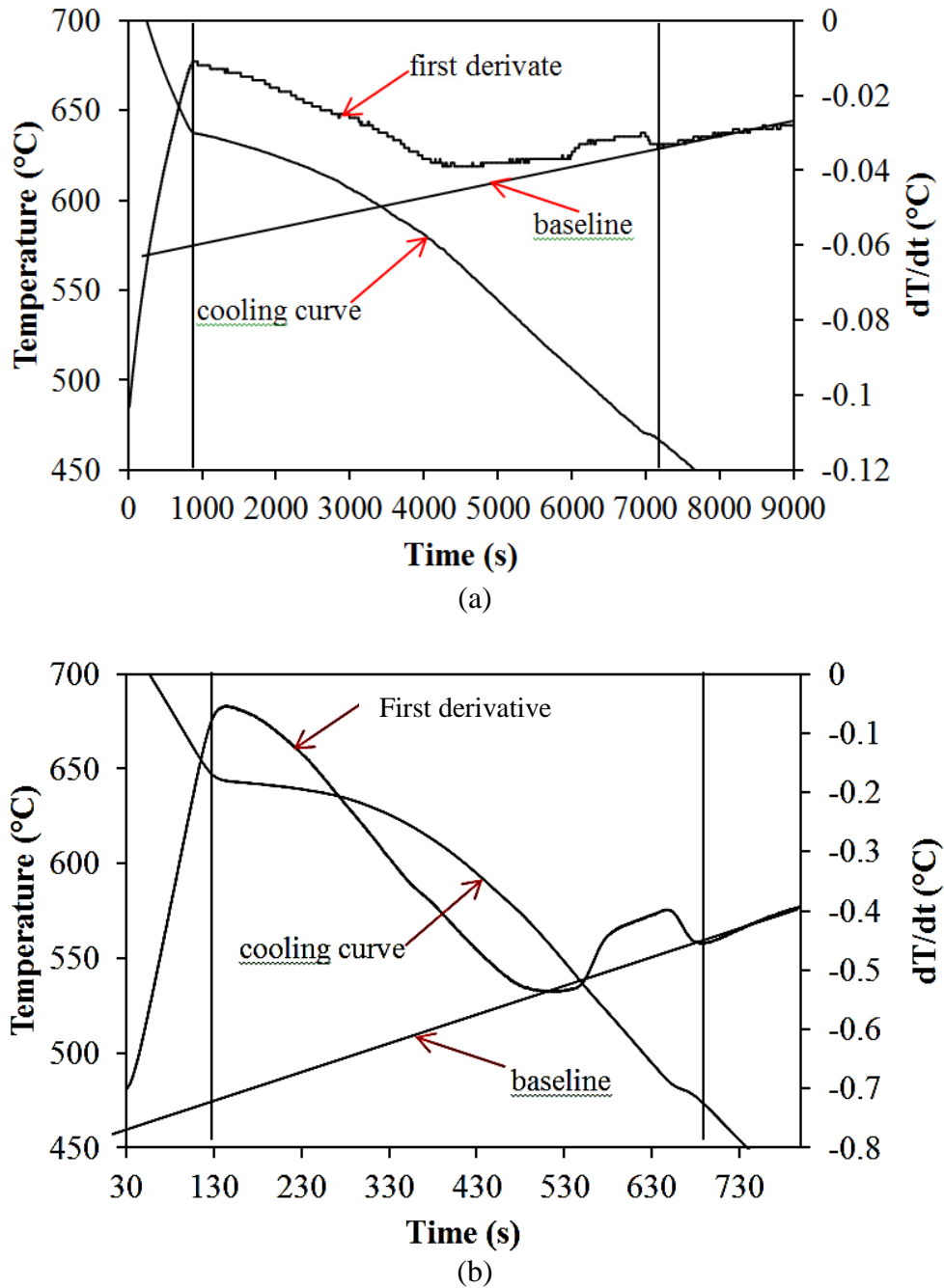
Figure 2. Thermal analysis results for (a) cooling rate 0.03°C/s (slow cooling rate) and for (b) cooling rate 0.4°C/s (higher cooling rate).

The calculated fraction solid versus temperature graph for both cooling rates are presented in Figure 3. The information in Figure 3 is particularly useful for determining the processing temperature settings for semi-solid metal processing. The results show that a suitable fraction solid (in the range of 30 to 70%) for SSM processing was in the temperature range of 610°C to 635°C. The results for the temperature difference

between the wall and center of the molten 7075 during solidification are shown in Figure 4 (a) for the slow cooling rate and Figure 4 (b) for the higher cooling rate. Vertical lines in these graphs represent the formation of DCP temperature and time. The DCP was determined by measuring the apparent temperature change between temperature at the center and wall. The DCP for the slow and the higher cooling rates occurred at time 2815.6s and 285.3s corresponding to temperatures of 615.2°C and 633.1°C respectively.
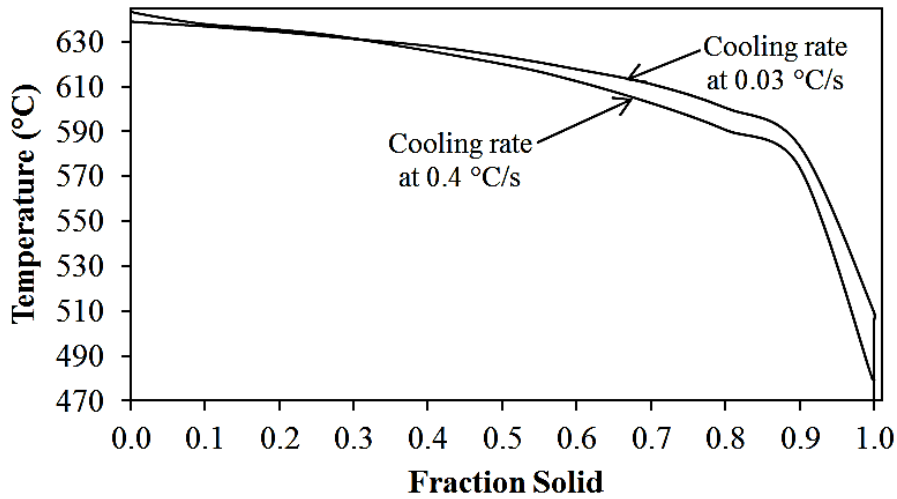
Figure 3. Calculated temperature-fraction solid relationships for both cooling rates.
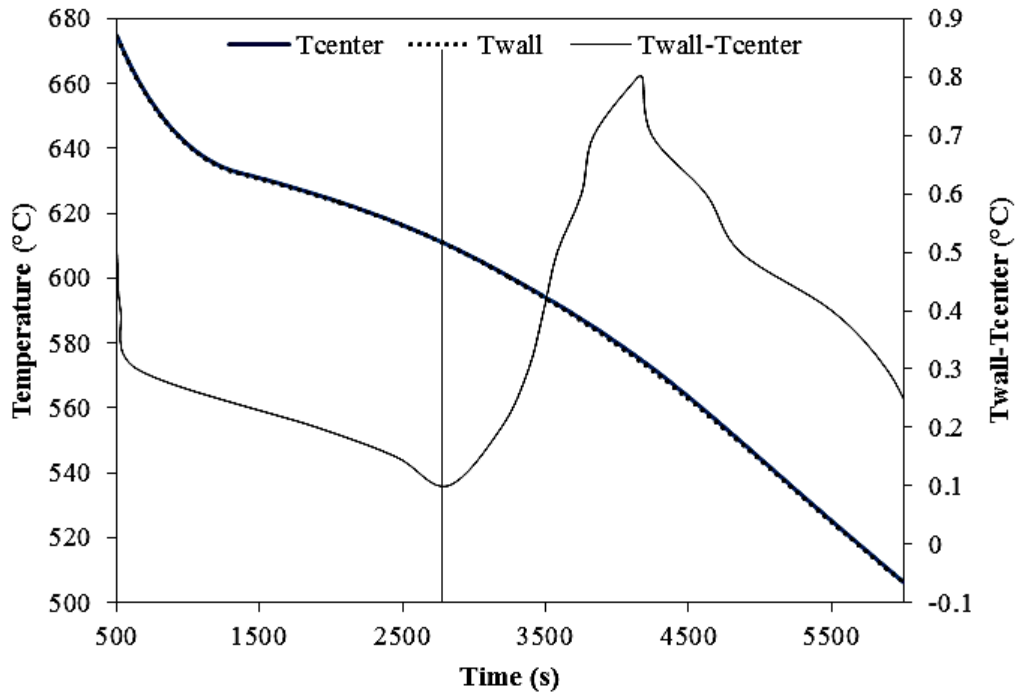
Figure 4 (a). Temperature difference between center and wall of the graphite crucible with slow cooling rate. The vertical line indicates formation temperature and time of DCP.
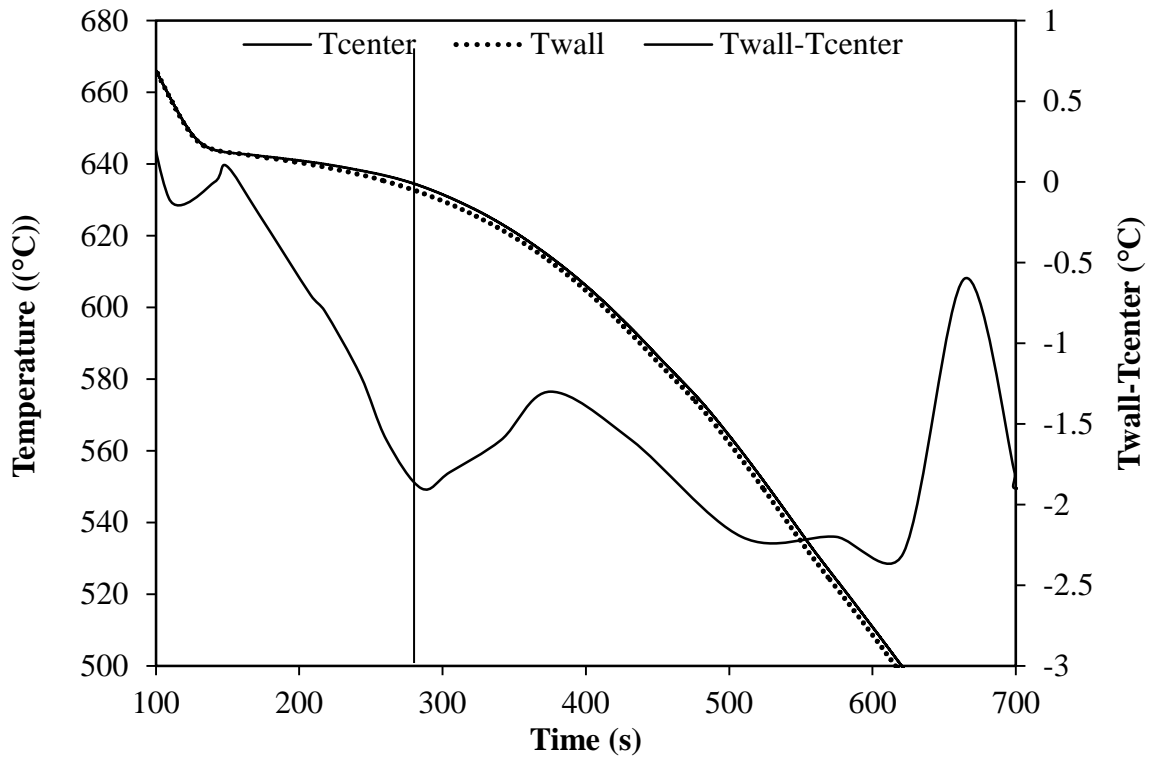
Figure 4 (b). Temperature difference between center and wall of the graphite crucible with higher cooling rate. The vertical line indicates formation temperature and time of DCP.

Microstructure Analysis

The microstructures for the starting material are shown in Figure 5. The grain structures were elongated and were un-recrystallized as shown by the contrast variations with the elongated grains. A higher magnification image is shown in Figure 5 (b) with a clearer microstructure feature.
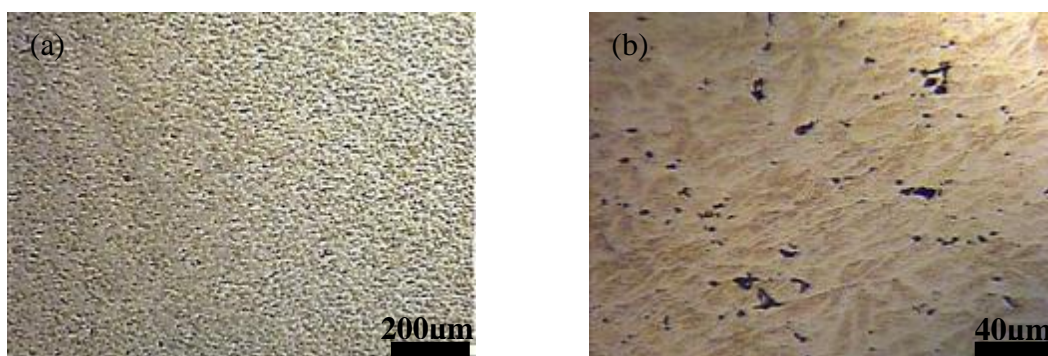
Figure 5. Microstructure for as-received aluminum 7075 with elongated and un-recrystallized structure for (a) low magnification (8x magnification) and (b) higher magnification (40x magnification).

The crossed section areas for microstructure samples and microstructure images for different cooling rate conditions are presented in Figure 6. The samples were crossed

crossed sectioned from three different locations as shown in Figure 6(a), Figure 6(b) and Figure 6(c). In order to assess the effects of cooling rate on the microstructure, qualitative comparison was used. The microstructures for the slow cooling rate condition are presented in Figure 6(d), Figure 6(e) and Figure 6(f), and the microstructures for the higher cooling rates are presented in Figure 6 (g - i).
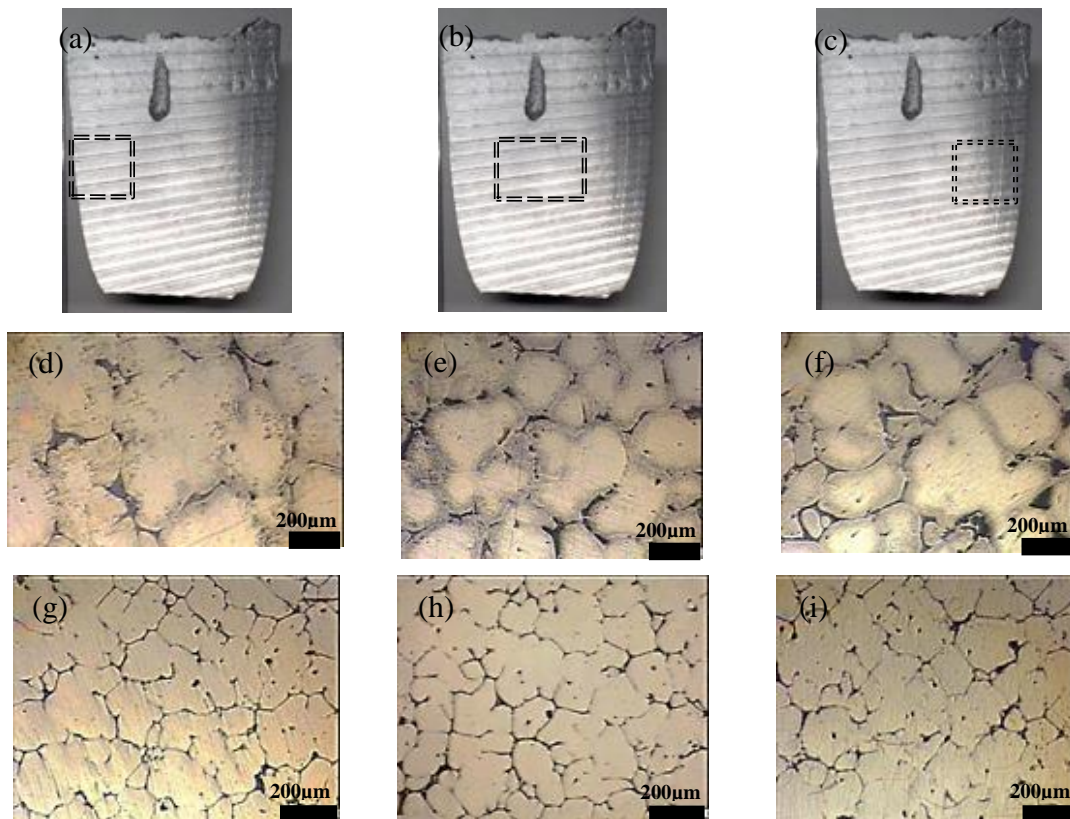
Figure 6. Crossed section area for solidified 7075 showing different locations used for microstructure analysis at (a) crucible wall (left), (b) center, and (c) crucible wall (right). The microstructural images for slow cooling rate at (d) crucible wall (right), (e) center, (f) crucible wall (left); and at higher cooling rate at (g) crucible wall (left), (h) center, and (i) crucible wall (right).

Effect of Cooling rate on Fraction Solid and DCP

In the current experimental work, the temperatures at which phase change occurred for 7075 were found to change by altering the cooling rate used. Eutectic and solidus temperatures were 470.2°C and 467.6°C for the slow cooling rate. The eutectic and solidus temperatures for the higher cooling rate were 482.7°C and 479.2°C respectively. The liquidus temperature for both cooling rates was not much affected with the different cooling rates used. The liquidus temperatures for the slow cooling rate and the higher cooling rate were 639.9°C and 643°C. Both the eutectic and solidus temperature formation were transformed near liquidus temperature for the higher cooling rate. In contrast, the formations of eutectic and solidus temperatures for the slow cooling rate occurred far from the liquidus temperature. The eutectic and solidus temperatures increased with the increment of the cooling rate. The fraction solid values were also

changed by use of different cooling rates. The difference between the fraction solid graph for slow cooling and for the higher cooling rate was apparent at the 0.7 fraction solid location (see Figure 3). In comparing these results with other reported results similar trends were found (Bäckerud et al., 1991). Possible explanations for the results were presented by Hosseini, Shabestari, and Gholizadeh (2013). The cooling rate shows a strong relationship with the formation of DCP. The DCP temperature for the slow cooling rate and the higher cooling rate occurred at 615.2°C and 633.1°C respectively, as shown in Figure 3. The formation of DCP was delayed with a slow cooling rate. The use of the higher cooling rate (in this work 0.4°C/s) accelerated formation of DCP and allowed it to occur close to the liquidus temperature. This was due to the growth rate of the dendrite arms increasing with the increasing cooling rate. This finding supports previous research linking cooling rate and DCP (Zeer, Pervukhin, & Zelenkova, 2011) .

Effect of Cooling Rate on Microstructure

The formation of microstructures were highly dependent on the cooling rate. The microstructures for the different cooling rates in Figure 6 shows that the higher cooling rate (0.4°C/s) was less spherical compared with microstructures for the slow cooling rate (0.03°C/s). The present findings seem to be consistent with other research which found that changes in the microstructure were mainly caused by using the different cooling rates (Bunck, Warnken, & Buhrig-Polaczek, 2010), however, the higher cooling rate and short solidification time reduce the grain size. The incremental cooling rate not only created finer microstructure but at the same time reduced the shape factor.

CONCLUSIONS

The thermal analysis with different cooling rates were successfully investigated. The temperatures at which material phase changes occurred changed significantly with the different cooling rates used. The eutectic and solidus temperature for a slow cooling rate (0.03°C/s) occurred at 470.2°C and 467.6°C, and for higher cooling rate (0.4°C/s) occurred at 482.7°C and 479.2°C respectively. The liquidus temperature for both cooling rates was not much affected by the variation in cooling rates. The DCP formation was delayed with the slow cooling rate and advanced with the higher cooling rate. This was due to the change of cooling rates affecting the solidification time and dendritic arm growth rate. The DCP was formed at a temperature of 615.2°C for the slow cooling rate, and at 633.1°C for the higher cooling rate. The different cooling rates also had a significant effect on features of the microstructure: a more spherical and globular microstructure formed at the slow cooling rate compared with the higher cooling rate.

ACKNOWLEDGEMENTS

REFERENCES

Box, G. E. P., & Draper, N. R. (1987). *Empirical model-building and response surfaces.* : New York: John Wiley & Sons.

Brabazon, D., Browne, D. J., & Carr, A. J. (2003). Experimental investigation of the transient and steady state rheological behaviour of al-si alloys in the mushy state. *Materials Science and Engineering A,* A356, 68-80.

Bunck, M., Warnken, N., & Buhrig-Polaczek, A. (2010). Microstructure evolution of rheo-cast a356 aluminium alloy in consideration of different cooling conditions by means of the cooling channel process. *Journal of Materials Processing Technology,* 210, 624-630.

Bäckerud, L., Chai, G., & Tamminen, J. (1991). *Solidification characteristics of aluminium alloys* (Vol. 2: Foundry Alloys.): University of Stockholm. .

Farahany, S., Bakhsheshi-Rad, H. R., Idris, M. H., Abdul Kadir, M. R., Lotfabadi, A. F., & Ourdjini, A. (2012). In-situ thermal analysis and macroscopical characterization of mg–xca and mg–0.5ca–xzn alloy systems *Thermochimica Acta,* 527, 180-189.

Guan, R. G., Zhao, Z. Y., Zhang, H., Lian, C., Lee, C. S., & Liu, C. M. (2012). Microstructure evolution and properties of mg–3sn–1mn (wt%) alloy strip processed by semisolid rheo-rolling. *Journal of Materials Processing Technology,* 212(6), 1430-1436.

Guo, H., Yang, X., Wang, J., Hu, B., & Zhu, G. (2010). Effects of rheoforming on microstructures and mechanical properties of 7075 wrought aluminium alloy. *Transactions of Nonferrous Metals Society of China,* 20, 355-360.

Hongwei Zhang, L. G., & Lina Guan, L. H. (2010). Effects of sic particle pretreatment and stirring parameters on the microstructure and mechanical properties of sicp/al-6.8mg composites fabricated by semi-solid stirring technique *Materials Science and Engineering A,* 526, 513-518.

Hosseini, V. A., Shabestari, S. G., & Gholizadeh, R. (2013). Study on the effect of cooling rate on the solidification parameters, microstructure, and mechanical properties of lm13 alloy using cooling curve thermal analysis technique. *Materials & Design,* 50, 7-14.

Kirkwood, H. (1994). Semisolid metal processing. *International Materials Reviews,* 39(5), 173-189.

Kiuchi, M. K. R. (2002). Mushy/semi-solid metal forming technology - present and future. *CIRP Annals - Manufacturing Technology,* 51(2), 653-670.

Spencer, D. B., Mehrabian, R., & Flemings, M. C. (1972). Rheological behaviour of sn-15 pct pb in the crystallization range. *Metallurgical Transactions,* 3, 1925-1932.

Vaneetveld, G., Rassili, A., Pierret, J. C., & Lecomte-Beckers, J. (2010). Conception of tooling adapted to thixoforging of high solid fraction hot-crack-sensitive aluminium alloys. *Transactions of Nonferrous Metals Society of China,* 20, 1712-1718.

Yang, B., Moa, W. M., & Song, X. J. (2014). Microstructure evolution of semi-solid 7075 al alloy slurry during temperature homogenization treatment. *Transactions of Nonferrous Metals Society of China,* 23, 3592-3597.

Zeer, G., Pervukhin, M., & Zelenkova, E. (2011). Effect of cooling rate on microstructure formation during crystallization of aluminum alloy 1417m. . *Metal Science and Heat Treatment,* 53(5-6), 210-212.

Zoqui, E. J., Paes, M., & Es-Sadiqi, E. (2002). Macro- and microstructure analysis of ssm a356 produced by electromagnetic stirring. *Journal of Materials Processing Technology,* 120(1-3), 365-373.